Geotech Geol Eng
https://doi.org/10.1007/s10706-021-01930-9

ORIGINAL PAPER

Numerical Investigation of Tunnel Face Stability Using Forepoling or Fiberglass Nails

M. Kavvadas · D. Georgiou · A. Kalos

Received: 8 May 2021 / Accepted: 1 July 2021

Abstract Pre-support of tunnel excavation faces using fiberglass nails or forepoling umbrellas aims to improve face stability in cases where an unsupported excavation face will develop uncontrollably large face extrusion, leading to face instability. The paper presents the results of a large set of parametric 3D numerical analyses of tunnel face excavation by the Finite Element Code Simulia Abaqus, using various degrees of reinforcement by fiberglass nails or forepoling umbrellas. The analyses use the average face extrusion as a measure of face stability, considering that face instability is associated with large face extrusions while the safety factor against face instability can be correlated with lower face extrusions in case of pre-supported tunnel faces. The results of the analyses are normalized and a set of semi-empirical formulae and design graphs are produced to calculate the safety factor of supported tunnel faces against instability and other useful quantities in tunnel design (average face extrusion, volume loss and deconfinement coefficient) as a function of ground strength, overburden depth and amount of face reinforcement. The analyses show that tunnel face reinforcement with FG nails is much more effective and less costly in securing face stability than the use of forepoling umbrellas. It is shown that even a coarse grid of FG nails can achieve better results than very heavy forepoling, and the difference in effectiveness is more pronounced in weaker ground and or deeper tunnels.

Keywords Tunnelling · Rockmechanics · Soilmechanics · Tunnel face stability · Forepoling umbrella · Fiberglass nailis

List of Symbols

A	Tunnel section area (m^2)
c	Soil cohesion (Mohr–Coulomb failure criterion)
D	Tunnel width (m)
E	Young modulus of the soil or rockmass
E_i	Intact rock Young modulus
GSI	Geomechanics Strength Index
H	Overburden depth measured from the tunnel axis up to the ground surface
L	Length of the tunnel core
m_b, s, a	Parameters of the Hoek–Brown failure criterion
p_o	Average overburden pressure at the tunnel axis (average of vertical and horizontal geostatic stresses).
SF	Safety factor of the tunnel face against instability
U_h	Average face extrusion

M. Kavvadas · D. Georgiou (✉) · A. Kalos
National Technical University of Athens, Athens, Greece
e-mail: dgeorgiou@mail.ntua.gr

M. Kavvadas
e-mail: kavvadas@central.ntua.gr

A. Kalos
e-mail: alkalos@central.ntua.gr

Published online: 08 July 2021

U_R	Radial convergence of the tunnel wall
V	Volume of the core, ahead of the tunnel face
VL	Volume loss = ΔV/V
K_o	Horizontal geostatic stress coefficient
ΔV	Reduction of V, due to tunnel wall convergence
α	Forepoling stiffness parameter
β	Fiber-Glass nail density parameter
Λ_f	Face stability parameter
λ	Deconfinement ratio
v	Poisson ratio of the ground
σ_{ci}	Intact rock strength
σ_{cm}	Ground strength (for soils and rockmasses)
ϕ	Soil friction angle (Mohr–Coulomb failure criterion)
Ω_f	Face extrusion parameter

1 Introduction

Controlling face stability is very important in tunnelling, as cases of face instability are frequent, severely affect the cost and construction schedule of tunnels and can damage surface structures and utilities in shallow urban tunnels. In mechanized tunnelling with active face pressure (e.g. EPB and Slurry TBMs), the risk of face instability is controlled by the applied face pressure, which is usually adjusted empirically using past performance in "similar" conditions. In tunnelling with conventional techniques (SCL/NATM), face stability is also assessed empirically in most cases, by subjective comparison of the excavation face with past behaviour of faces under "similar" conditions (i.e., avoiding past failures), occasionally by simplified limit equilibrium analyses (e.g. Leca and Dormieux 1990; Anagnostou and Kovári 1996; Kim and Tonon 2010), and rarely by numerical analysis or systematic measurements of axial face movements (face extrusion). When the risk of face instability is considered unacceptable in SCL/NATM tunnels, the size of the excavation face is reduced or active face support measures are applied, such as fiber-glass (FG) nailing, forepoling, or even leaving a ground wedge on the face. In practically all cases, the capacity of these measures is selected empirically: standard size forepoles (114/100 mm spaced at 0.50 m over a 120-degree crown arch) or FG nails at a "reasonable" spacing (one anchor per 2.5–5 m^2 of face area).

Forepoling umbrellas (FPU) include a set of stiff steel pipes installed ahead of the tunnel face, at the perimeter of the crown of the tunnel. The forepoles are 12 m long steel tubes of diameter 60–170 mm, installed with a typical spacing S = 40–60 cm, at a slight inclination (5 to 7 degrees) with respect to the tunnel axis, and cover the upper part of the tunnel wall, at an angle of about 120 degrees. The steel pipes need to overlap along a length of 3—5 m in order to provide continuous face support as the tunnel face advances. The vertical load from the ground above the forepoles is carried by bending of the forepoles and is transferred to their rear support (steel sets of the temporary lining) and front end support (fixation in the ground ahead of the extruding face core), thus reducing the vertical pressure on the extruding core ahead of the tunnel face. The reduction of the ground load on the extruding core reduces face extrusion and radial wall convergence, thus improving face stability. The reduction of tunnel wall convergence by means of forepoling umbrellas has been studied by several researchers, using 2D and 3D numerical analyses (e.g. Oke et al. 2016).

Fiberglass nails (FGN) have also been used for the reinforcement of tunnel faces. FGN are inserted in holes drilled on the tunnel face at a regular grid, which are then fully cement grouted to ensure full bonding of the nails with the surrounding ground. Their length must be sufficient to permit anchoring beyond the extruding core ahead of the tunnel face. As FG nails are installed in regular distances as the tunnel face advances, a length overlap is crucial in controlling their effectiveness. FGN provide an equivalent pressure on the tunnel face equal to their total tensile force over the face area. Tension of the FGN develops by the tendency of the tunnel face to extrude; thus the FGN reduce face extrusion and radial wall convergence, improving face stability. Peila (1994) reports that use of fiberglass nails can reduce tunnel face deformations by up to 40%. Yoo (2002) based on 3D numerical analyses reports that the use of fiberglass nails can reduce tunnel face deformations by up to 70%. Ng and Lee (2002), based on 3D numerical analyses, also highlight the importance of face reinforcement by fiberglass nails in reducing tunnel face deformation and settlements at ground surface.

The effectiveness of various face support measures in improving tunnel face stability has been studied by several researchers, such as: Lunardi and Bindi 2000; Kamata and Mashimo 2003; Anagnostou and Serafeimidis 2007; Kavvadas and Prountzopoulos 2009; Juneja et al. 2010; Dias 2011; Anagnostou and Perazzelli 2015 and Perazzelli and Anagnostou 2020. Despite these efforts, the design of face support measures still remains largely empirical. The main reason of the extensive empiricism in assessing face stability, is that quantitative assessment of face stability requires the definition of a suitable "safety factor", and its calculation using complex three-dimensional (3D) numerical analyses with realistic constitutive models and suitably measured/estimated ground parameters. Although seemingly trivial, even the definition of a "safety factor" for face stability analyses is not always straight forward, let alone its numerical calculation. Georgiou et al (2021) have investigated face stability in tunnels with unsupported faces by performing a large set of parametric 3D finite element analyses of the excavation face. In this investigation, the "safety factor" against face instability was defined and calculated in various ground and tunnel conditions.

The present study extends the methods developed by Georgiou et al (2021), to include tunnel faces supported with forepoling umbrellas (FPU) and fiberglass nails (FGN). The investigation method is similar to that used for unsupported tunnel faces: a large set of parametric 3D finite element analyses of the excavation face is performed using the Finite Element Code Simulia Abaqus. In each case of ground conditions and overburden depth, a number of analyses are performed using various densities of FGN reinforcement or forepoling umbrellas to calculate the average face extrusion, which is obviously lower than that of the corresponding unsupported face. The results of the analyses are normalized and a set of semi-empirical formulae are produced to calculate the safety factor of the supported excavation face against instability and other useful quantities in tunnel design (average face extrusion, volume loss and deconfinement coefficient). As these assessments are based and extend on quantities defined in the paper by Georgiou et al (2021) for unsupported tunnel faces, a summary of these findings is given in the next section.

2 Face Stability in Tunnels with Unsupported Face

Georgiou et al (2021) investigated face stability in tunnels with unsupported faces by performing 120 3D finite element analyses of the excavation face with the Finite Element Code Simulia Abaqus, varying ground conditions (in soils and weak rockmasses) and overburden depths. The analyses calculate the axial displacement (face extrusion) at all integration points on the tunnel face. These values are averaged over the tunnel face to give an "average face extrusion" (U_h) which is then normalized by the tunnel width (D) and a modulus-to-depth factor (E/p_o) to give the dimensionless "face extrusion parameter" (Ω_f):

$$\Omega_f = \left(\frac{U_h}{D}\right)\left(\frac{E}{p_o}\right) \tag{1}$$

where E is the elastic Young modulus of the ground (soil or rockmass) and $p_o = 0.5(1 + K_o)\gamma H$ is the average overburden pressure at the tunnel axis (average of vertical and horizontal geostatic stresses).

The 120 values of the calculated face extrusion parameter (Ω_f) were then plotted against various forms of strength-to-stress ratio, in search of an optimal correlation. The optimal correlation was achieved for the following dimensionless "face stability parameter" (Λ_f):

$$\Lambda_f = 3.8\left(\frac{\sigma_{cm}}{\gamma H\sqrt{1 + (2/3)K_o}}\right)\left(\frac{H}{D}\right)^{0.35} \tag{2}$$

which combines ground strength (σ_{cm}), average overburden stress (p_o) and tunnel width (D). Georgiou et al. (2021) have shown that this parameter can best describe the relevant parameters of the tunnel excavation face (face extrusion, volume loss, radial wall displacement, deconfinement ratio and safety factor against stability), in the sense that the calculated values in the FE analyses correlate well with the corresponding parameter (Λ_f). Control analyses have shown that the above formula can also be used in various tunnel shapes, including separate excavation of the top heading of a tunnel, via an equivalent tunnel size parameter D = 1.15 sqrt(A), where A is the section area of the tunnel or phase.

In soils, the ground strength was calculated by the Uniaxial Compressive Strength using the Mohr–Coulomb failure criterion:

$$\sigma_{cm} = 2c\tan(45^\circ + \varphi/2) \tag{3a}$$

In weak or very fractured rockmasses, yielding was modelled by the Hoek–Brown failure criterion. In this case, "rockmass strength" (σ_{cm}) and "rockmass modulus" (E) were calculated by the following empirical formulae, in terms of the Geological Strength Index—GSI (Hoek and Diederichs 2006; Litsas et al 2017):

$$\sigma_{cm} = 0.02\sigma_{ci}\exp\left(\frac{GSI}{25.5}\right) \tag{3b}$$

$$E = E_i\left[0.02 + \frac{1}{1+\exp[(60-GSI)/11]}\right] \tag{3c}$$

In an unsupported tunnel face, the optimal correlation between face extrusion (Ω_f) and face stability parameter (Λ_f) is given by the formula:

$$\Omega_f = 1.4\Lambda_f^{-1.2} \tag{4}$$

This formula can be used to estimate the face extrusion parameter (Ω_f) and, via Eq. 1, calculate the average face extrusion (U_h) for an unsupported tunnel face with given (Λ_f), i.e., a tunnel of size (D), overburden depth (H), in ground with strength (σ_{cm}).

The above correlation shows that, when $\Lambda_f < 1$, the face extrusion parameter (Ω_f) starts to increase rapidly, with values $\Omega_f > 1.4$. Thus, the condition $(\Lambda_f)_{lim} = 1$, corresponding to face extrusion $(\Omega_f)_{lim} = 1.4$, was considered as limiting face stability in unsupported tunnel faces.

At limiting face stability, Eqs. (4), (1) and (2) give the limiting face extrusion and limiting ground strength in unsupported tunnel faces:

$$(\Omega_f)_{lim} = 1.4 \Rightarrow \left(\frac{U_h}{D}\right)_{lim} = 1.4\left(\frac{p_o}{E}\right) \tag{5a}$$

$$(\sigma_{cm})_{lim} = 0.263\gamma H\sqrt{1+(2/3)K_o}\left(\frac{D}{H}\right)^{0.35} \tag{5b}$$

where $(\sigma_{cm})_{lim}$ is the lowest ground strength to ensure limiting stability of an unsupported face for a tunnel with width (D) and overburden depth (H).

Since stable tunnel faces correspond to $\Lambda_f > 1$ and unstable faces to $\Lambda_f < 1$, the safety factor (SF) of a tunnel face (either unsupported or supported) can be defined by the ratio of the face stability parameter (Λ_f), defined by Eq. (2) and depending only on tunnel geometry and ground strength, to the corresponding limiting value $(\Lambda_f)_{lim}$ (corresponding to face extrusion $(\Omega_f)_{lim} = 1.4$ for any tunnel face):

$$SF = \frac{\Lambda_f}{(\Lambda_f)_{lim}} \tag{6}$$

For an unsupported tunnel face, $(\Lambda_f)_{lim} = 1$ and thus (using Eqs. 6 and 2):

$$SF_o = 3.8\left(\frac{\sigma_{cm}}{\gamma H\sqrt{1+(2/3)K_o}}\right)\left(\frac{H}{D}\right)^{0.35} \tag{7}$$

For supported tunnel faces, $(\Lambda_f)_{lim} < 1$, due to the beneficial effect of the face support measures. Thus, the reduction of the limiting face stability parameter by the face support measures, increases the safety factor of an initially unstable unsupported tunnel face ($\Lambda_f < 1$), possibly rendering the tunnel face stable (if $SF > 1$). The present paper calculates the decrease of the limiting face stability parameter by the face support measures, and thus calculates the safety factor of supported tunnel faces (from Eq. 6).

For unsupported tunnel faces, the face stability parameter (Λ_f) is also used to calculate the radial displacement (U_R) of the tunnel wall at the excavation face:

$$\frac{U_R}{D} = 1.75\left(\frac{p_o}{E}\right)(\Lambda_f)^{-1.2} \tag{8}$$

and the corresponding volume loss (VL), caused by (U_R) which "squeezes" the core ahead of the tunnel face, giving face extrusion (U_h). Volume loss (VL) is defined as the reduction (ΔV) of the volume (V) of the extrusion core ahead of the tunnel face per unit volume of the core ($VL = \Delta V/V$):

$$VL = 1.83\left(\frac{p_o}{E}\right)(\Lambda_f)^{-1.2} \tag{9}$$

Finally, the face stability parameter (Λ_f) is used to calculate the deconfinement ratio (λ) at the tunnel face by the formula:

$$\lambda = 0.25 + 0.75\exp(-\Lambda_f/2) \tag{10}$$

At limiting face stability ($\Lambda_f = 1$), the deconfinement ratio at the tunnel face is: $\lambda_{lim} = 0.70$.

In supported tunnel faces, quantities (U_R), (VL) and (λ) can be calculated by the same formulae, replacing (Λ_f) by the corresponding limiting value $(\Lambda_f)_{lim}$ which depends on the face support measures.

3 Numerical Investigation of Supported Tunnel Faces

The present study extends the above methods to include tunnel faces supported with forepoling umbrellas (FPU) and fiber-glass nails (FGN). The investigation method includes a large set of parametric 3D finite element analyses of the excavation face, using the Finite Element Code Simulia Abaqus. Figure 1 shows the shape of the tunnel section used in the analyses.

Figure 2 shows the finite element mesh used in the analyses, with eight-node hexahedral finite elements. Due to symmetry about the vertical plane, only the left half of the model is analysed. Following a sensitivity analysis, the extent of the finite element mesh is sufficiently large (at least 3.5D in each direction) to minimize boundary effects in all directions. The conditions on the tunnel face are assessed after an initial tunnel advance by 5 to 7 D from the left (start) edge of the FE mesh, leaving a clear distance 3.5 to 5.5 D from the right end boundary (ahead of the tunnel face). For overburden depths $H > 3D$, additional overburden is simulated as a surface pressure, because ground stiffness and strength in this zone does not influence tunnel excavation. The tunnel section is excavated in a single phase (full face excavation) with excavation steps of 1 m (equal to the size of the elements in the axial direction). In each excavation step, a relatively stiff (30 cm thick) shotcrete liner is installed on the tunnel wall (full ring) 2 m behind the excavation face. The shotcrete liner is modelled as linearly elastic 4-noded shell elements, with a relatively low concrete modulus equal to E = 15 GPa to account for concrete setting time during tunnel advance. Parametric analyses have shown that the thickness and stiffness of the shotcrete shell do not influence the magnitude of face extrusion (which is of main interest in the present study).

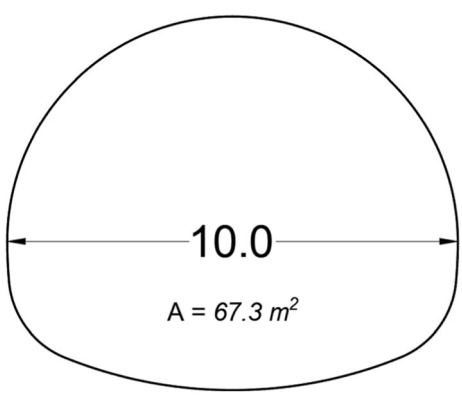

Fig. 1 Cross-section of the oval-shaped tunnel used in the finite element analyses. Width D = 10 m, section area A = 67.3 m^2

Forepoling tubes are modelled as horizontal beams spanning the tunnel crown at an angle 120 degrees (60 degrees at each side of the crown) with spacing S = 0.50 m. The beams are very long, to avoid the need to install new forepoles every several meters of tunnel advance. Parametric analyses have shown that the replacement of the slightly inclined forepoles with horizontal beams does not influence the accuracy of the results. The beams are modelled as elastic—perfectly plastic with elastic modulus E = 200 GPa, Poisson ratio ν = 0.25 and yield stress 235 MPa. The following six types of forepoling beams are used in the analysis (the lighter tubes aimed to confirm that the numerical solution converges to the unsupported face condition when the forepoling stiffness tends to zero):

The moment of inertia (I) per meter width was calculated for forepole spacing S = 0.50 m as:

$$I = \frac{\pi}{64\,S}\left(d_o^4 - d_i^4\right) \quad in\ \mathrm{mm}^4/\mathrm{mm} \tag{11}$$

Table 1 also shows the corresponding values of a forepoling stiffness parameter (α), defined as:

$$\alpha = 0.05\,I^{0.125} \quad in\ (\mathrm{mm})^{3/8} \tag{12a}$$

Fiberglass nails are modelled as horizontal truss elements, evenly spaced on the tunnel face. The nails are very long, to avoid the need to install new nails every several meters of tunnel advance. The nails are modelled as elastic—perfectly plastic with elastic modulus E = 40 GPa, Poisson ratio ν = 0.30, yield load $P_{u,FG}$ = 200 kN and mobilisation factor 50% of the yield load (F = 2). Three nail densities (n/A) are examined: one anchor per 1.0, 2.0 and 4.0 m^2 of tunnel face area. For each anchor density, the following dimensionless FGN density parameter (β) is defined:

$$\beta = 1.2\left(\frac{n\,P_{u,FG}}{F\,A\,p_a}\right)^{0.35} \tag{12b}$$

where (n) is the number of FG nails on tunnel face (A), $P_{u,FG}$ = 200 kN is the yield load of the nails, F = 2 is the nail force mobilisation factor (FE analyses show that FG nails develop tension equal to about 50% of the yield strength) and p_a is the atmospheric pressure

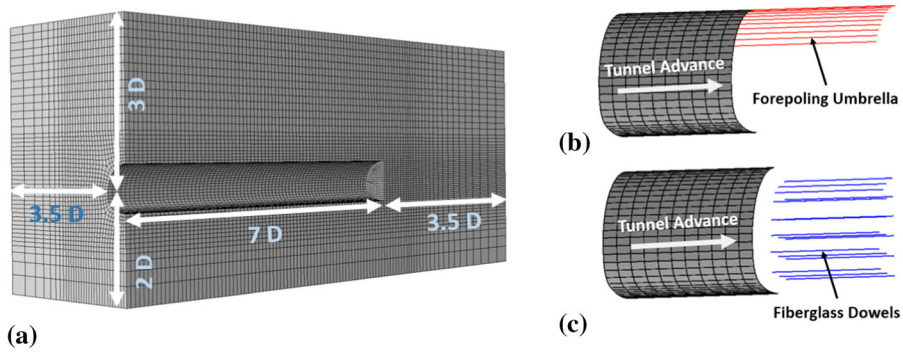

Fig. 2 Finite element mesh used in the analyses. The case shown corresponds to overburden depth H = 3D = 30 m. The right part of the figure shows the model of the forepoles (horizontal beams) and the fiberglass nails (horizontal truss elements)

Table 1 Forepoling tubes used in the analyses

Outside diameter do (mm)	Wall thickness t (mm)	Moment of inertia I (mm^4/m)	Forepole stiffness parameter a ($mm^{3/8}$)	Section modulus W (cm^3/m)	Yield moment My (kNm/m)
20	1	5.40	0.062	0.54	0.13
25	2	19.26	0.072	1.54	0.36
34	3	70.85	0.085	4.17	0.98
70	7	1391.8	0.124	39.76	9.34
114.3	7	6820.7	0.151	119.35	28.05
168.3	7	23,115.8	0.176	274.70	64.55

(p_a = 100 kPa) used for normalisation purposes. The three nail densities examined (n/A = one nail per 1.0, 2.0 and 4.0 m^2 of tunnel face area) give density parameters β = 1.20, 0.94 and 0.74, respectively.

The numerical analyses include shallow tunnels in soils and deep tunnels in weak or heavily fractured rockmass. In each ground/overburden combination, a number of analyses are performed using various degrees of reinforcement by fiberglass nails (three nail densities) or forepoling umbrellas (six forepoling types) to calculate the average face extrusion of the supported tunnel face and compare it to the corresponding values of the unsupported face.

Shallow tunnels:

In shallow tunnels, two cases of overburden depth (measured from the tunnel axis up to the ground surface), are examined: H = 20 m (H/D = 2) and H = 30 m (H/D = 3), with ground unit weight γ = 20 kN/m^3 and two cases of the horizontal geostatic stress coefficient: K_o = 0.5 and 1.0 (to include the effect of the horizontal stress ratio). The ground is relatively stiff elastic—perfectly plastic, with elastic modulus (E), Poisson ratio v = 0.33, yielding according to the Mohr–Coulomb criterion (c = cohesion, φ = friction angle). The assumption of a linearly elastic—perfectly plastic material is a necessary simplifying assumption for the present parametric analyses, since a more advanced model (such as strain hardening or softening) introduces additional parameters to be investigated, making the

Table 2 Sets of ground parameters used in the analyses of shallow tunnels

c (kPa)	*φ* (°)	σ_{cm} (kPa)	*E* (MPa)
20.0	22.5	59.9	80
20.0	25.0	62.8	100
25.0	25.0	78.5	120
30.0	25.0	94.2	150
30.0	30.0	103.9	170
50.0	30.0	173.2	200

parameter combinations intractable. Table 2 shows the six sets of ground parameters used in the analyses.

According to the Mohr–Coulomb failure criterion, the ground strength (σ_{cm}) is equal to the Uniaxial Compressive Strength defined by Eq. (3a). The E-modulus is rather large, because it represents the elastic response before plastic yielding. After yielding, stiffness is drastically reduced by the accumulation of plastic strains. The total number of numerical analyses of shallow tunnels was 24 (two tunnel depths, two K_o values and six sets of material parameters).

Deep tunnels:

In deep tunnels, three overburden depths are examined: H = 100 m, 150 m and 200 m in weak or heavily fractures rockmass with unit weight γ = 25 kN/m^3, horizontal geostatic stress coefficient K_o = 0.5 and 1.0 (two cases), intact rock properties σ_{ci} = 10 MPa and E_i = 2 GPa, Poisson ratio v = 0.33 and Geological Strength Index in the range GSI = 25 to 45 (three cases). The rockmass was assumed linearly elastic—perfectly plastic, yielding according to the Generalised Hoek–Brown failure criterion (Hoek et al 2002) with various parameters (m_b, s, a). Table 3 shows the three sets of rockmass parameters used in the parametric analyses.

The "rockmass strength" (σ_{cm}) and "rockmass modulus" (E) for the various GSI values are calculated by formulae (3b). The total number of numerical analyses for the deep tunnels was 18 (three tunnel depths, two K_o values, and three sets of material parameters).

The total number of numerical analyses with supported face was (24 + 18) × 6 = 252 with forepoling and (24 + 18) × 3 = 126 with face nailing, plus (24 + 18) = 42 cases without face reinforcement.

Each numerical analysis calculates the axial displacement (face extrusion) at all integration points on the tunnel face. These values are averaged over the tunnel face to give an "average face extrusion" (U_h) which is then normalized by the tunnel width (D) and a modulus-to-depth factor (E/p_o) to give the dimensionless "face extrusion parameter" (Ω_f) defined in Eq. (1). The face extrusion parameter of the unsupported tunnel face is denoted as (Ω_{fo}) and the reduction of the face extrusion parameter with respect to the unsupported face is:

$$\Delta\Omega_f = \Omega_{fo} - \Omega_f \rightarrow \frac{\Delta\Omega_f}{\Omega_{fo}} = 1 - \frac{\Omega_f}{\Omega_{fo}} \tag{13}$$

Table 3 Sets of rockmass parameters used in the analyses of deep tunnels

GSI	m_b	*s*	*a*	σ_{cm} (MPa)	*E* (MPa)
25	0.687	2.4×10^{-4}	0.531	0.53	119.7
35	0.981	7.3×10^{-4}	0.516	0.79	226.8
45	1.403	2.0×10^{-3}	0.508	1.17	447.3

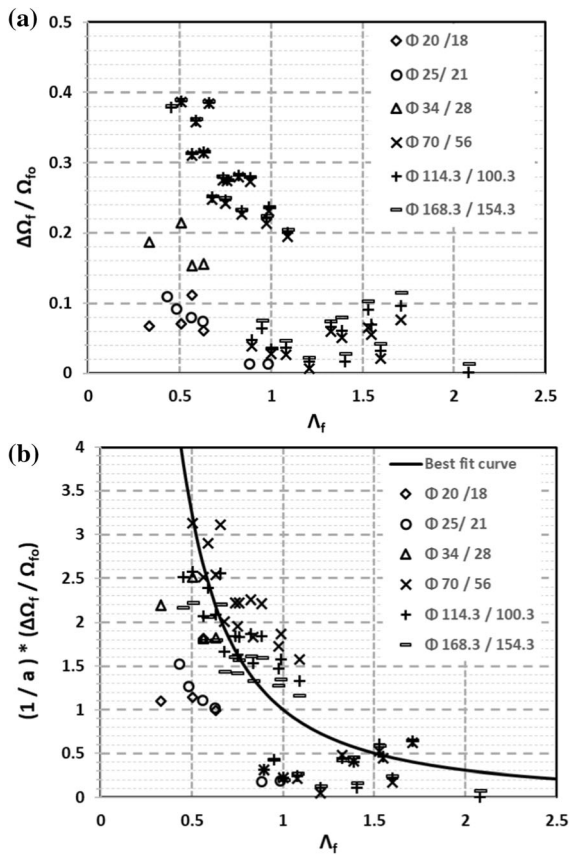

Fig. 3 **a** Effect of forepoling stiffness on the reduction of the average face extrusion, plotted versus the face stability parameter (Λ_f). **b** Effect of forepoling stiffness on the reduction of the average face extrusion, plotted versus the face stability parameter (Λ_f). The vertical axis is normalized with an optimally selected forepoling stiffness parameter (α)

4 Analysis of Face Support with Forepoling Umbrellas (FPU)

Figure 3a plots the calculated decrease of the face extrusion parameter ($\Delta\Omega_f$), normalized with the corresponding face extrusion of the unsupported face (Ω_{fo}), versus the face stability parameter (Λ_f) (defined by Eq. 2), for tunnel faces supported with six types of forepoles. Stiffer forepoles (with higher moment of inertia I—see Table 1) reduce face extrusion more, while forepoles of very small stiffness give very small extrusion reductions, comparable with the unsupported face ($\Delta\Omega_f = 0$), confirming the robustness of the numerical algorithm. Larger values of the face stability parameter (Λ_f), corresponding to better ground strength/overburden stress combinations, cause smaller face extrusions for all forepoling types. For $\Lambda_f > 2$, face extrusion is very small even in unsupported faces ($\Omega_{fo} < 0.5$) and thus the additional decrease of face extrusion due to face reinforcement is negligible for all types of forepoles, rendering the use of face support by forepoling as practically useless.

In Fig. 3b, the vertical axis is normalized with a forepoling stiffness parameter (α), defined by Eq. (12a). Parameter (α) was optimally selected to reduce the scatter of the face extrusion reductions ($\Delta\Omega_f$) shown in Fig. 3a for the commonly used forepoles ($d_o > 70$ mm); most of the data points deviating a lot from the best fit curve correspond to small diameter forepoles, not used in practical applications. The best fit curve in Fig. 3b can be expressed by the formula (combined with Eq. 4):

$$\left(\frac{1}{\alpha}\right)\left(\frac{\Delta\Omega_f}{\Omega_{fo}}\right) = \left(\Lambda_f\right)^{-1.7} \Rightarrow \Delta\Omega_f = 1.4\alpha\left(\Lambda_f\right)^{-2.9} \tag{14a}$$

Using this formula, the face extrusion parameter (Ω_f) of the supported tunnel faces can be expressed as:

$$\Omega_f = \Omega_{fo}\left[1 - \alpha\left(\Lambda_f\right)^{-1.7}\right] \Rightarrow \Omega_f = 1.4\left(\Lambda_f\right)^{-1.2}\left[1 - \alpha\left(\Lambda_f\right)^{-1.7}\right] \tag{14b}$$

Using Eq. (1), the above formula can be used to calculate the average face extrusion (U_h) for various ground strength/overburden stress combinations and various forepoling stiffnesses (i.e., values of the α parameter):

$$\frac{U_h}{D} = 1.4\left(\frac{p_o}{E}\right)\left(\Lambda_f\right)^{-1.2}\left[1 - \alpha\left(\Lambda_f\right)^{-1.7}\right] \tag{14c}$$

Figure 4 plots the relationship of the face extrusion parameter (Ω_f) versus (Λ_f), for selected values of forepoling stiffness parameter (α), using Eq. (14b). Appreciable reduction of face extrusion occurs for $\Lambda_f < 1$, where the unsupported face has limiting stability, with increasing values of the forepoling stiffness parameter (α).

Figure 5 plots the limiting value of the face stability parameter $(\Lambda_f)_{lim}$ versus the forepoling stiffness parameter (α), from Eq. (14b) by setting $\Omega f = 1.4$ (limiting face stability). The parameter $(\Lambda_f)_{lim}$ is the value of (Λ_f) causing face extrusion $\Omega_f = 1.4$ which, by analogy to the unsupported tunnel faces (Eq. 5), corresponds to limiting unstable tunnel faces. Thus, Fig. 5 gives the values of (Λ_f) where face instability occurs, with increasing stiffness of the forepoles. Stiffness values larger than $\alpha = 0.20$ correspond to forepoling diameters larger than those typically used (up to about 200 mm) and thus the achieved improvement is only theoretical. For typical diameters of the forepoling tubes (d = 60–120 mm), the parameter $\alpha = 0.10$–0.15 which gives $(\Lambda_f)_{lim} = 0.90$–0.80 (i.e., 10–20% reduction of the limiting face stability parameter with respect to the corresponding value of the unsupported face).

Using Eq. (2), and the limiting values of (Λ_f) shown in Fig. 5, Eq. (15) gives the limiting value of ground strength $(\sigma_{cm})_{lim}$, which is the lowest ground strength

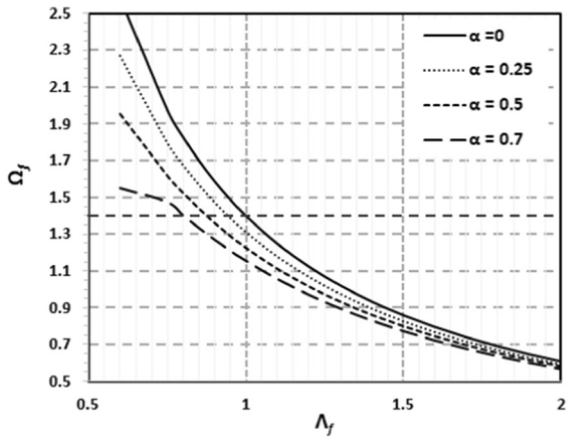

Fig. 4 Relationship of (Ω_f) versus (Λ_f) for selected values of the forepoling stiffness parameter (α). The thick black line corresponds to the unsupported tunnel face ($\alpha = 0$). The dashed line ($\Omega_f = 1.4$) corresponds to limiting face stability

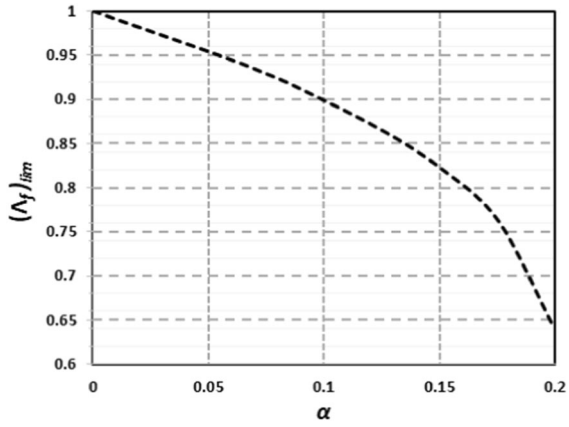

Fig. 5 Correlation of the limiting value of the face stability parameter (Λ_f) versus the forepoling stiffness parameter (α). Values of $\alpha > 0.20$ are not examined as they correspond to unrealistically stiff forepoling tubes (d > 200 mm)

to ensure limiting face stability for a given tunnel size (D), overburden depth (H) and face support with forepoling stiffness parameter (α).

$$(\sigma_{cm})_{\lim} = 0.263\,\gamma H\sqrt{1+(2/3)K_o}\left(\frac{D}{H}\right)^{0.35}(\Lambda_f)_{\lim} \tag{15}$$

Figure 6 plots the safety factor (SF) of the tunnel face (defined by Eq. 6) versus the face stability parameter (Λ_f), for selected values of the forepoling stiffness parameter (α). For each value of (α), the limiting parameter $(\Lambda_f)_{\lim}$ is obtained from Fig. 5. The thick black line corresponds to the unsupported tunnel face, where $(\Lambda_f)_{\lim} = 1$. For typical diameters of the forepoling tubes (α = 0.10–0.15), the safety factor of the excavation face increases by 15–20%.

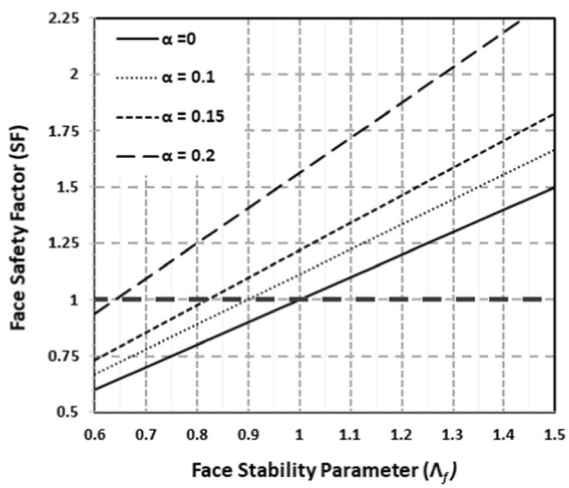

Fig. 6 Correlation of the Safety Factor (SF) against face stability with the stability parameter (Λ_f) for selected values of the forepoling stiffness parameter (α)

5 Analysis of Face Support with Fiberglass Nails (FGN)

Figure 7a plots the calculated decrease of the face extrusion parameter ($\Delta\Omega_f$), normalized with the corresponding face extrusion of the unsupported face (Ω_{fo}), versus the face stability parameter (Λ_f) (defined by Eq. 2) for tunnel faces supported with three

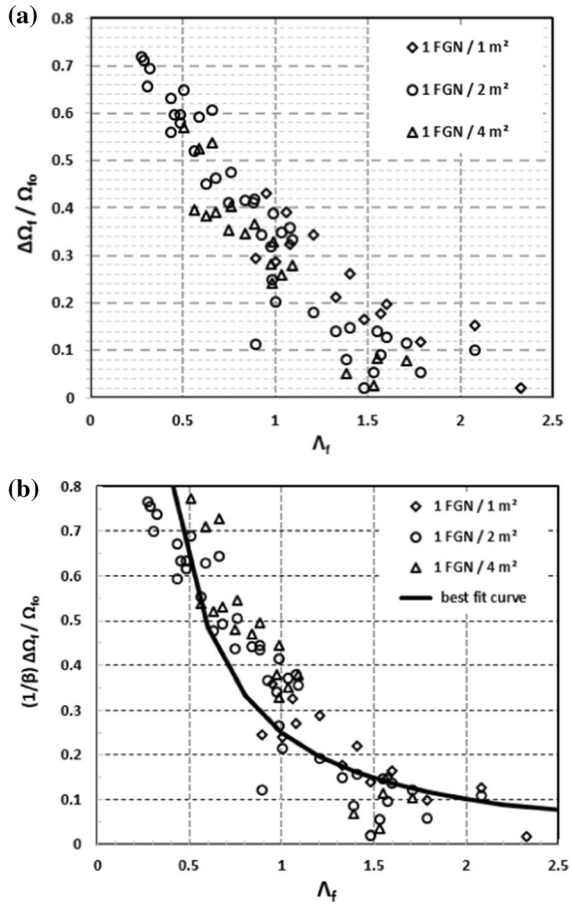

Fig. 7 **a** Effect of Fiber-Glass Nail (FGN) density on the reduction of the average face extrusion, plotted versus the face stability parameter (Λ_f). **b** Effect of Fiber-Glass Nail (FGN) density on the reduction of the average face extrusion, plotted versus the face stability parameter (Λ_f). The vertical axis is normalized with an optimally selected FGN density parameter (β)

densities of Fiber-Glass nails (FGN). Nail grids of higher density reduce face extrusion more, while larger values of the face stability parameter, corresponding to better ground strength/overburden stress combinations, cause smaller face extrusions for all grid densities. For $\Lambda_f > 2$, face extrusion is very small even in unsupported faces ($\Omega_{fo} < 0.5$) and thus the additional decrease of face extrusion due to face reinforcement is negligible for all FG grid densities, rendering the use of FG nails as practically useless.

In Fig. 7b, the vertical axis is normalized with a FGN density parameter (β), defined by Eq. (12b). Parameter (β) was optimally selected to reduce the scatter of the face extrusion reductions ($\Delta\Omega_f$) in Fig. 7a. The best fit curve can be expressed by the formula (combined with Eq. 4):

$$\left(\frac{1}{\beta}\right)\left(\frac{\Delta\Omega}{\Omega_{fo}}\right) = 0.25\left(\Lambda_f\right)^{-1.30} \Rightarrow \Delta\Omega_f = 0.35\beta\left(\Lambda_f\right)^{-2.5} \quad (16a)$$

Using this formula, the face extrusion parameter (Ω_f) of the supported tunnel faces can be expressed as:

$$\Omega_f = \Omega_{fo}\left[1 - 0.25\beta\left(\Lambda_f\right)^{-1.3}\right] \Rightarrow \Omega_f = 1.4\left(\Lambda_f\right)^{-1.2}\left[1 - 0.25\beta\left(\Lambda_f\right)^{-1.3}\right] \quad (16b)$$

Using Eq. (1), the above formula can be used to calculate the average face extrusion (U_h) for various ground strength/overburden stress combinations and various FGN densities (i.e., values of the β parameter):

$$\frac{U_h}{D} = 1.4\left(\frac{p_o}{E}\right)\left(\Lambda_f\right)^{-1.2}\left[1 - 0.25\beta\left(\Lambda_f\right)^{-1.3}\right] \quad (16c)$$

Using Eq. (16b), Fig. 8 plots the relationship of the face extrusion parameter (Ω_f) versus (Λ_f), for selected values of FGN densities (β). Appreciable reduction of face extrusion occurs for $\Lambda_f < 1$, where the unsupported face has limiting stability. For FGN density $\beta > 0.675$, the tunnel face is stable for practically any ground strength/overburden stress combinations (i.e., any value of Λ_f).

Figure 9 plots the limiting value of the face stability parameter $(\Lambda_f)_{lim}$ versus the FGN density parameter (β). The parameter $(\Lambda_f)_{lim}$ is the value of (Λ_f) causing face extrusion $\Omega_f = 1.4$ which, by analogy to the unsupported tunnel faces (Eq. 5), corresponds to unstable tunnel faces. Thus, Fig. 9 gives the limiting values of (Λ_f) where face instability occurs, with

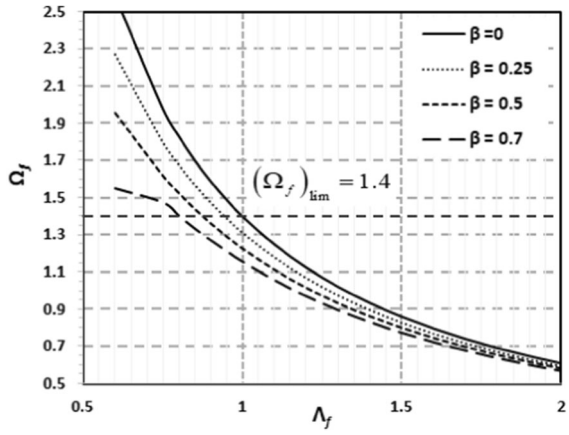

Fig. 8 Relationship of (Ω_f) versus (Λ_f) for selected values of FGN density parameter (β). The thick black line corresponds to the unsupported tunnel face (β = 0). The dashed line (Ω_f = 1.4) corresponds to limiting face stability

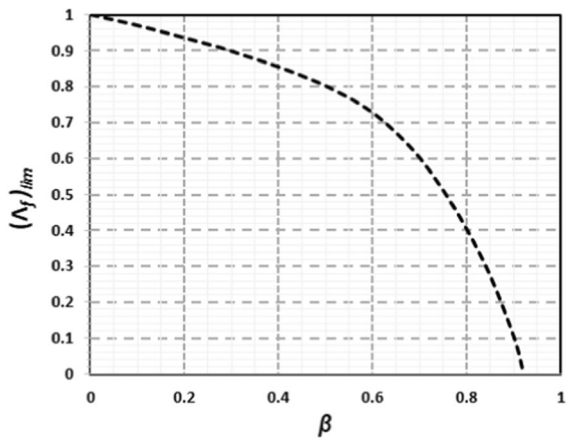

Fig. 9 Correlation of the limiting value of the face stability parameter (Λ_f) versus the FGN density parameter (β)

increasing FGN density. For FGN densities $\beta > 0.92$, the tunnel face is stable for practically any ground strength/overburden stress combinations (i.e., any value of Λ_f). For typical FG nail densities (one nail per 12.5 ÷ 4 m^2 of tunnel face), the FG density parameter β = 0.50–0.74, which gives $(\Lambda_f)_{lim}$ = 0.80–0.50 (i.e., 20–50% reduction with respect to the unsupported face). Comparing these reductions with those of face support by forepoling tubes (10–20% reduction with respect to the unsupported face), it is concluded that the lightest FG nail density (1 nail per 12.5 m^2 of face area) achieves the same improvement of face stability as the heaviest

forepoling tubes (diameter about 200 mm), giving a clear advantage to face support by FG nails.

Using Eq. (2), and the limiting values of (Λ_f) shown in Fig. 9, Eq. (17) gives the limiting value of ground strength (σ_{cm})$_{lim}$, which is the lowest ground strength to ensure limiting face stability for a given tunnel size (D), overburden depth (H) and face support with FGN density parameter (α).

$$(\sigma_{cm})_{\lim} = 0.263\,\gamma H\sqrt{1+(2/3)K_o}\left(\frac{D}{H}\right)^{0.35}(\Lambda_f)_{\lim} \tag{17}$$

Figure 10 plots the safety factor (SF) of the tunnel face (defined by Eq. 6) versus the face stability parameter (Λ_f), for selected values of the FGN density parameter (β). The thick black line corresponds to the unsupported tunnel face (where SF = 1 for Λ_f = 1). For FGN densities $\beta > 0.92$, the tunnel face is stable (SF > 1) for practically any value of Λ_f.

6 Other Results for Supported Tunnel Faces

By analogy to the unsupported tunnel faces (Eqs. 8, 9, 10) the following equations give the the radial displacement (U_R) of the tunnel wall, the volume loss (VL) and the deconfinement ratio (λ) at the excavation face, for tunnels with supported faces, in terms of the face stability parameter (Λ_f) and the corresponding limiting value (Λ_f)$_{lim}$ which depends on the type and capacity of the face support (Fig. 5 for forepoles and Fig. 9 for FG nails):

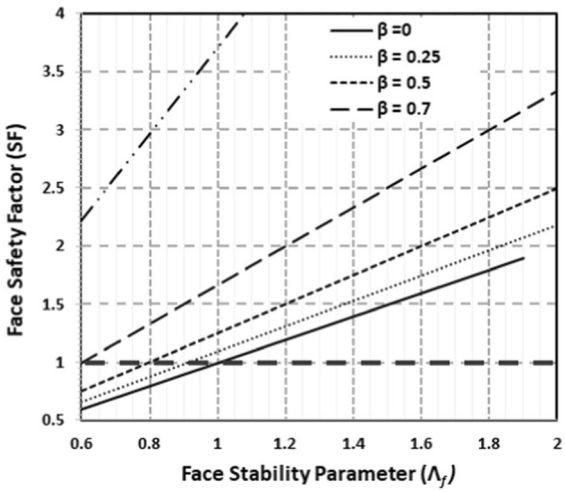

Fig. 10 Correlation of the Safety Factor (SF) against face stability with the stability parameter (Λ_f) for selected values of the FGN density parameter (β)

$$\frac{U_R}{D} = 1.75\left(\frac{p_o}{E}\right)\left(\frac{\Lambda_f}{(\Lambda_f)_{\lim}}\right)^{-1.2} \tag{18}$$

$$VL = 1.83\left(\frac{p_o}{E}\right)\left(\frac{\Lambda_f}{(\Lambda_f)_{\lim}}\right)^{-1.2} \tag{19}$$

$$\lambda = 0.25 + 0.75\,\exp\left(-\frac{1}{2}\frac{\Lambda_f}{(\Lambda_f)_{\lim}}\right) \tag{20}$$

7 Application Example

The above formulae, produced by normalizing the results of many parametric finite element analyses of tunnel faces supported with forepoling or FG nails, can assist in the selection of suitable face support measures in unstable or marginally stable tunnel faces. Some typical examples are given below, with the objective to compare the effectiveness of forepoling versus FG nails in improving face stability.

A tunnel with width D = 10 m and section area A = 67.3 m^2 is excavated at depth H = 250 m in a heavily fractured rockmass, with intact strength σ_{ci} = 10 MPa, intact modulus Ei = 2.5 GPa and GSI = 25. The ground has unit weight γ = 23 kN/m^3 και K_o = 0.6.

The calculated rockmass strength and modulus are (Eqs. 3b and 3c): σ_{cm} = 533 kPa, E = 150 MPa, p_o = 4600 kPa and (p_o/E) = 4.6/150 = 0.0307. The face stability parameter is (Eq. 2): $\Lambda_f = 0.92 < 1$, indicating that the unsupported tunnel face is unstable, with safety factor (Eq. 6 or 7): SF_o = 0.92.

For the unsupported tunnel face, the radial displacement (U_R) of the tunnel wall at the excavation face is (Eq. 8): U_R/D = 6%, the volume loss is (Eq. 9): VL = 6.2% and the deconfinement ratio at the tunnel face is (Eq. 10): λ = 0.724.

If the tunnel face is supported with heavy forepoling tubes of diameter 114/100 mm, spaced every 50 cm on a top arch of 120 degrees (22 tubes in total), the forepoling stiffness parameter is (Eq. 12a): α = 0.151 which corresponds to a limiting value of the face stability parameter (Fig. 5) (Λ_f)$_{lim}$ = 0.821

and the safety factor of the tunnel face is (Eq. 6): SF = 0.919/0.821 = 1.12 > 1 (stable face). For this configuration, the radial displacement (U_R) of the tunnel wall at the excavation face is (Eq. 18): U_R/D = 4.7%, the volume loss is (Eq. 19): VL = 4.9% and the deconfinement ratio at the tunnel face is (Eq. 20): $\lambda = 0.679$. These values are a little lower than the corresponding values of the unsupported tunnel face, showing that forepoling has some effect in improving face stability conditions.

If the tunnel face is supported with very heavy forepoling tubes of diameter 168/154 mm, spaced every 50 cm on a top arch of 120 degrees (again 22 tubes in total), the forepoling stiffness parameter is $\alpha = 0.176$ which which corresponds to a limiting value of the face stability parameter $(\Lambda_f)_{lim} = 0.761$ and the safety factor of the tunnel face is SF = 1.21 > 1. This is the largest possible safety factor, since the heaviest possible forepoling was used. For this configuration, the radial displacement (U_R) of the tunnel wall at the excavation face is U_R/D = 4.3%, the volume loss is VL = 4.5% and the deconfinement ratio at the tunnel face is $\lambda = 0.66$. These values are very little lower than those corresponding to the 114/100 mm forepoling, indicating that even very heavy forepoling does not increase the safety factor of the tunnel face significantly ($SF_o = 0.92$ of the unsupported face, increased to SF = 1.21 for the most heavy forepoling).

Alternatively, if the tunnel face is supported with only n = 8 FG nails (1 nail every 8.5 m^2 of face area, Pu = 200 kN and F = 2), the FG density parameter is (Eq. 12b): $\beta = 0.569$, which gives limiting value of the face stability parameter (Fig. 9) $(\Lambda_f)_{lim} = 0.75$ and the safety factor of the tunnel face is (Eq. 6): SF = 0.919/0.75 = 1.22 > 1. For this configuration, the radial displacement (U_R) of the tunnel wall at the excavation face is (Eq. 18): U_R/D = 4.2%, the volume loss is (Eq. 19): VL = 4.4% and the deconfinement ratio at the tunnel face is (Eq. 20): $\lambda = 0.657$. These face parameters, achieved with only 8 FG nails, are similar to the result achieved with the heaviest possible forepoling (22 tubes of 168/154 mm). Obviously, the cost of the FG nails is much lower than the corresponding cost of the forepoling.

If the tunnel face is supported with n = 14 FG nails (1 nail every 4.8 m^2 of face area, Pu = 200 kN and F = 2), the FG density parameter is $\beta = 0.693$, which gives limiting value of the face stability parameter $(\Lambda_f)_{lim} = 0.61$ and the safety factor of the tunnel face is SF = 0.919/0.61 = 1.51. For this configuration, the radial displacement (U_R) of the tunnel wall at the excavation face is U_R/D = 3.3%, the volume loss is VL = 3.4% and the deconfinement ratio at the tunnel face is $\lambda = 0.60$. These face parameters, achieved with 14 FG nails, are much better than the result achieved with the heaviest possible forepoling (22 tubes of 168/154 mm), where the safety factor is only SF = 1.21 at a much larger cost.

The difference in effectiveness of the FG nails is even larger in weak ground, where even the heaviest forepoling cannot achieve face stability. For example, in a tunnel excavated in heavily fractured rockmass with intact strength $\sigma_{ci} = 8$ MPa, intact modulus Ei = 2 GPa, GSI = 20 at depth H = 180 m, the safety factor of the unsupported face is: $SF_o = 0.75$ (unstable face). With the most heavy forepoling (168/154 mm spaced at 50 cm), the safety factor increases to SF = 0.98 and the face is still marginally stable. If the tunnel face is supported with FG nails, the same improvement (SF = 0.98) can be achieved with only 8 FG nails (one nail every 8.5 m^2 of tunnel face). With 13 nails (one nail every 5.2 m^2 of tunnel face) the safety factor is increased to SF = 1.21 and with 22 nails (one nail every 3 m^2 of tunnel face) the safety factor is increased to SF = 1.97. In the last case, the radial displacement (U_R) of the tunnel wall at the excavation face is U_R/D = 2.8%, the volume loss is VL = 2.9% and the deconfinement ratio at the tunnel face is $\lambda = 0.53$. The advantage of FG nails in improving face stability in very poor rockmasses, compared to the use of forepoling umbrellas, is evident.

8 Conclusions

Georgiou et al (2021) have investigated stability of unsupported tunnel faces by parametric 3D finite element analyses using the Finite Element (FE) Code Simulia Abaqus. The present study extends these methods to include tunnel faces supported with forepoling umbrellas (FPU) and fiber-glass nails (FGN). In each case of ground conditions and overburden depth, a number of FE analyses are performed using various densities of FGN reinforcement or forepoling umbrellas to calculate the average face extrusion, which is obviously lower than that of

the corresponding unsupported face. The analyses use the average face extrusion as a measure of face stability, considering that face instability is associated with large face extrusions while the safety factor against face instability can be correlated with lower face extrusions in case of pre-supported tunnel faces. The results of the analyses are normalized and a set of semi-empirical formulae and design graphs are produced to calculate the safety factor of supported tunnel faces against instability and other useful quantities in tunnel design (average face extrusion, volume loss and deconfinement coefficient) as a function of ground strength, overburden depth and amount of face reinforcement.

The analyses show that tunnel face reinforcement with FG nails is much more effective and less costly in securing face stability than the use of forepoling umbrellas. It is shown that even a coarse grid of FG nails can achieve better results than very heavy forepoling, and the difference in effectiveness is more pronounced in weaker ground and or deeper tunnels.

Acknowledgements The present work is part of the Ph.D. thesis research of Mr. D. Georgiou. It was supported by scholarship funding from the Alexander S. Onassis Public Benefit Foundation and the Evgenides Foundation.

References

Anagnostou G, Kovári K (1996) Face stability conditions with earth-pressure-balanced shields. Tunn Undergr Space Technol 11(2):165–173

Anagnostou G, Perazzelli P (2015) Analysis method and design charts for bolt reinforcement of the tunnel face in cohesive-frictional soils. Tunn Undergr Space Technol 47:162–181

Anagnostou G, Serafeimidis K (2007) The dimensioning of tunnel face reinforcement. In: Underground space–the 4th dimension of metropolises. ITA World Tunnel Congress, Prague (pp 291–296)

Carranza-Torres C, Alonso E, Alejano LR, Varas F, Fdez-Manin G (2002) Elasto-plastic analysis of deep tunnels in brittle rock using a scaled form of the Mohr-Coulomb failure criterion. In: Proceedings of the 5th North American rock mechanics symposium and the 17th tunnelling association of Canada conference, NARMS-TAC, Toronto, Canada, ed. Hammah et al (pp 283–293)

Dias D (2011) Convergence-confinement approach for designing tunnel face reinforcement by horizontal bolting. Tunn Undergr Space Technol 26(4):517–523

Georgiou D, Kalos A, Kavvadas M (2021) Numerical investigation of face stability in unsupported both shallow and deep tunnels (Submitted for publication at the Journal of Geotechnical and Geological Engineering)

Hoek E, Diederichs MS (2006) Empirical estimation of rock mass modulus. Int J Rock Mech Min Sci 43(2):203–215

Hoek E, Carranza-Torres C, Corkum B (2002) Hoek-Brown failure criterion-2002 edition. Proc NARMS-Tac 1(1):267–273

Juneja A, Hegde A, Lee FH, Yeo CH (2010) Centrifuge modelling of tunnel face reinforcement using forepoling. Tunn Undergr Space Technol 25(4):377–381

Kamata H, Mashimo H (2003) Centrifuge model test of tunnel face reinforcement by bolting. Tunn Undergr Space Technol 18(2–3):205–212

Kavvadas M, Prountzopoulos G (2009) 3D Analyses of tunnel face reinforcement using fiberglass nails. In: Eur: tun 2009 conference. Bochum

Kim SH, Tonon F (2010) Face stability and required support pressure for TBM driven tunnels with ideal face membrane—drained case. Tunn Undergr Space Technol 25(5):526–542

Leca E, Dormieux L (1990) Upper and lower bound solutions for the face stability of shallow circular tunnels in frictional material. Geotechnique 40(4):581–606

Litsas D, Sitarenios P, Kavvadas M (2017) Effect of the face support pressure on tunnelling-induced ground movement. In: World tunnel congress 2017: surface challenges–underground solutions»

Lunardi P (2008) Design and construction of tunnels: analysis of controlled deformations in rock and soils (ADECO-RS). Springer Science & Business Media

Lunardi, Bindi R (2000) The evolution of reinforcement of the advance core using fiberglass elements for short and long term stability of tunnels under difficult stress-strain conditions: design, technologies and operating methods. Prog Tunn After 309–322

Ng CWW, Lee GT (2002) A three-dimensional parametric study of the use of soil nails for stabilising tunnel faces. Comput Geotech 29(8):673–697

Oke J, Vlachopoulos N, Diederichs MS (2016) Semi-analytical model for umbrella arch systems employed in squeezing ground conditions. Tunn Undergr Space Technol 56:136–156

Peila D (1994) A theoretical study of reinforcement influence on the stability of a tunnel face. Geotech Geol Eng 12(3):145–168

Perazzelli P, Anagnostou G (2020) Optimization of the tunnel face bolt reinforcement. Tunnels and underground cities: engineering and innovation meet archaeology, architecture and art: volume 4: ground improvement in underground constructions, 1438

Prountzopoulos G (2012) Investigation of the excavation face stability in shallow tunnels. National Technical University, Geotechnical Division, Athens (in Greek)

Yoo C (2002) Finite-element analysis of tunnel face reinforced by longitudinal pipes. Comput Geotech 29(1):73–94

Terms and Conditions

Springer Nature journal content, brought to you courtesy of Springer Nature Customer Service Center GmbH (“Springer Nature”).
Springer Nature supports a reasonable amount of sharing of research papers by authors, subscribers and authorised users (“Users”), for small-scale personal, non-commercial use provided that all copyright, trade and service marks and other proprietary notices are maintained. By accessing, sharing, receiving or otherwise using the Springer Nature journal content you agree to these terms of use (“Terms”). For these purposes, Springer Nature considers academic use (by researchers and students) to be non-commercial.
These Terms are supplementary and will apply in addition to any applicable website terms and conditions, a relevant site licence or a personal subscription. These Terms will prevail over any conflict or ambiguity with regards to the relevant terms, a site licence or a personal subscription (to the extent of the conflict or ambiguity only). For Creative Commons-licensed articles, the terms of the Creative Commons license used will apply.
We collect and use personal data to provide access to the Springer Nature journal content. We may also use these personal data internally within ResearchGate and Springer Nature and as agreed share it, in an anonymised way, for purposes of tracking, analysis and reporting. We will not otherwise disclose your personal data outside the ResearchGate or the Springer Nature group of companies unless we have your permission as detailed in the Privacy Policy.
While Users may use the Springer Nature journal content for small scale, personal non-commercial use, it is important to note that Users may not:

1. use such content for the purpose of providing other users with access on a regular or large scale basis or as a means to circumvent access control;
2. use such content where to do so would be considered a criminal or statutory offence in any jurisdiction, or gives rise to civil liability, or is otherwise unlawful;
3. falsely or misleadingly imply or suggest endorsement, approval , sponsorship, or association unless explicitly agreed to by Springer Nature in writing;
4. use bots or other automated methods to access the content or redirect messages
5. override any security feature or exclusionary protocol; or
6. share the content in order to create substitute for Springer Nature products or services or a systematic database of Springer Nature journal content.

In line with the restriction against commercial use, Springer Nature does not permit the creation of a product or service that creates revenue, royalties, rent or income from our content or its inclusion as part of a paid for service or for other commercial gain. Springer Nature journal content cannot be used for inter-library loans and librarians may not upload Springer Nature journal content on a large scale into their, or any other, institutional repository.
These terms of use are reviewed regularly and may be amended at any time. Springer Nature is not obligated to publish any information or content on this website and may remove it or features or functionality at our sole discretion, at any time with or without notice. Springer Nature may revoke this licence to you at any time and remove access to any copies of the Springer Nature journal content which have been saved.
To the fullest extent permitted by law, Springer Nature makes no warranties, representations or guarantees to Users, either express or implied with respect to the Springer nature journal content and all parties disclaim and waive any implied warranties or warranties imposed by law, including merchantability or fitness for any particular purpose.
Please note that these rights do not automatically extend to content, data or other material published by Springer Nature that may be licensed from third parties.
If you would like to use or distribute our Springer Nature journal content to a wider audience or on a regular basis or in any other manner not expressly permitted by these Terms, please contact Springer Nature at

onlineservice@springernature.com